This is the accepted version of the following article: [Qu Z, Gong T, Wang XY, Li QQ, Wang T. Stiffness and strength demands for pin-supported walls in RC moment frames. ***Journal of Structural Engineering, ASCE***, DOI: 10.1061/(ASCE)ST.1943-541X.0002758. This article may be used for non-commercial purposes.

Stiffness and Strength Demands for Pin-Supported Walls in Reinforced Concrete Moment Frames

Zhe Qu[1*], Ting Gong[2], Xiaoyue Wang[3], Qiqi Li[4], Tao Wang[5]

[1] Professor, Ph.D., Institute of Engineering Mechanics, China Earthquake Administration, Yanjiao, Hebei 065201, China. Corresponding author. Email: quz@iem.ac.cn
[2] P.E., China Architecture Design & Research Group, Beijing, China
[3] Graduate student, Institute of Engineering Mechanics, China Earthquake Administration, Hebei, China.
[4] P.E., China Institute of Building Standard Design & Research, Beijing, China.
[5] Professor, Ph.D., Institute of Engineering Mechanics, China Earthquake Administration, Hebei, China.

Abstract: Criteria are proposed for determining the stiffness and strength demands for the seismic design of pin-supported walls in multi-story reinforced concrete moment-resisting frames. A plasticity ratio and a global stiffness ratio are introduced to evaluate the effect of pin-supported walls in mobilizing the seismic capacity of the moment-resisting frame. Incremental dynamic analyses of 4-, 8- and 12-story prototype moment-resisting frames equipped with pin-supported walls of various stiffness ratios show that a constant stiffness ratio of two can generally ensure a global plastic mechanism to form in a moment-resisting frame no matter if the frame is a strong column-weak beam one or not. By mobilizing more structural elements to contribute to the earthquake resistance, the pin-supported walls also increase the lateral strength of the structure. Higher mode vibrations have a major effect on the strength demand for pin-supported walls. Simple criteria are also developed for estimating the strength demands for the purpose of preliminary design of pin-supported walls. The same methods for determining the stiffness and strength demands for pin-supported walls are also applicable to other strong spine systems.
Keywords: pin-supported wall, reinforced concrete frame, strong spine system, stiffness ratio, plasticity ratio, higher mode vibration

1. Introduction

Vertical continuous stiffness is essential in spreading the lateral force and deformation among the individual stories of a building and thus in avoiding drift concentration and a consequential weak story collapse. As compared to columns in either moment-resisting or gravity frames (MacRae et al 2004), structural walls that are continuously configured along the full height of a building or across multiple stories would provide much greater vertical continuous stiffness, which can eliminate the weak story mechanism in the building (Paulay and Priestley 1992). Numerical analysis has shown that walls that are hinged at the base appeared to be a more effective solution to strengthening moment-resisting frames than conventional fixed-base walls. Hinged walls can considerably reduce maximum story drift demands and lead to a more uniform distribution of story drifts over the height of a building (Alavi and Krawinkler, 2004).

Following a similar idea, a retrofitting plan consisting of pin-supported walls (PS walls hereinafter) and steel dampers was proposed and implemented in an 11-story steel reinforced concrete frame that was built in the 1970s in Japan (Wada et al 2009, Qu Z et al 2012, Qu Z et al 2015). Six post-tensioned concrete walls that rest on mechanical pin bearings were attached to the existing structure along its perimeter to spread the lateral drift among the stories. Shear-type steel dampers were installed along both sides of each wall to increase the energy dissipation during earthquakes and thus to reduce the seismic response to the building. In addition to the seismic retrofitting purpose, PS walls can also be used in new construction. A typical configuration is shown in Figure 1, in which the lateral load on the floor is transferred by collectors at each floor level to the PS walls. The walls can sway laterally around the pin bearing at the base with the moment-resisting frame, making its story-by-story drift distribution more uniform. Dampers along both sides of the wall would take full advantage of the vertical relative displacement between the wall and the frame to maximize the energy dissipation.

The use of a strong spine, such as a PS wall to spread lateral drift and thus to avoid weak story failure under earthquakes has also attracted increasing attentions in steel constructions. A dual buckling restrained braced (BRB) frame system was proposed in the early 2000s to mitigate the story drift concentration in BRB frames (Tremblay and Merzouq 2004). A vertical truss alongside a bay with BRBs was developed so that the structure remains fully elastic under a design basis earthquake to force the vibration of the building to approach its first vibration mode (Figure 2(a)). A similar system was implemented in a 23-story steel braced building in Osaka, Japan, in the late 1990s (Aoki et al 1998). The same concept was later revisited and investigated under different names, such as a series of strong back systems (Lai and Mahin 2015) and a BRB mask system (Panian et al 2015). Following Takeuchi and Suzuki (2015), who applied buckling restrained columns for warehouse racks, Tremblay et al (2004) proposed a flexural braced frame system (Figure 2(b)), which also incorporates an elastic vertical truss for drift control. The system was implemented in a 5-story steel moment frame in Japan (referred to as a controlled spine frame by Takeuchi et al (2015)) and was also studied in China (Wu and Lu 2015). By adding vertical ties to connect the ends of shear links between floors to each other in an eccentrically braced frame (Figure 2(c)), tied braced frames are also equipped with strong spines that consists of vertical elastic braced frames (Rossi 2007, Tremblay et al 2014). A pivoting spine, which is a core wall resting on a friction pendulum, was used to seismically

retrofit a steel moment-resisting frame in the U.S. (Janhunen 2013, Figure 2(d)). The idea of using a core, either a vertical truss or a concrete wall, to mitigate story drift concentration was also extended to concentrically braced frames (Qu et al 2014, Pollino et al 2017, Slovenec et al, 2017). A recent state-of-the-art review of strong back systems in steel constructions is included in Liu (2017) (Liu 2017).

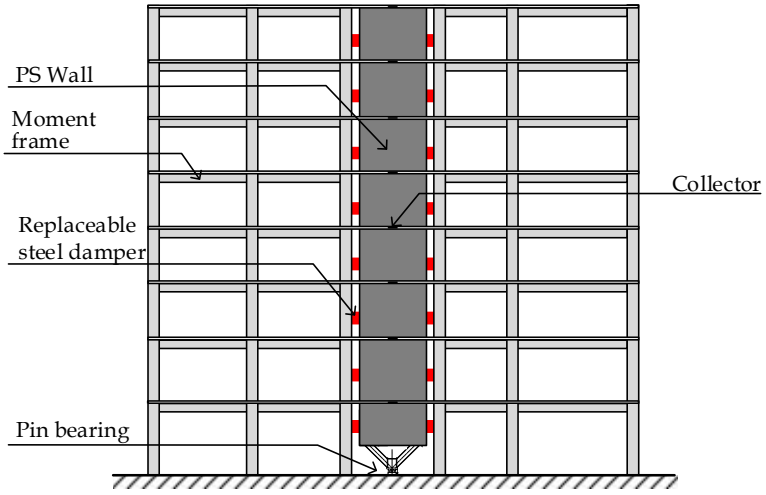

Figure 1. Example of a configuration of pin-supported walls in an RC moment-resisting frame.

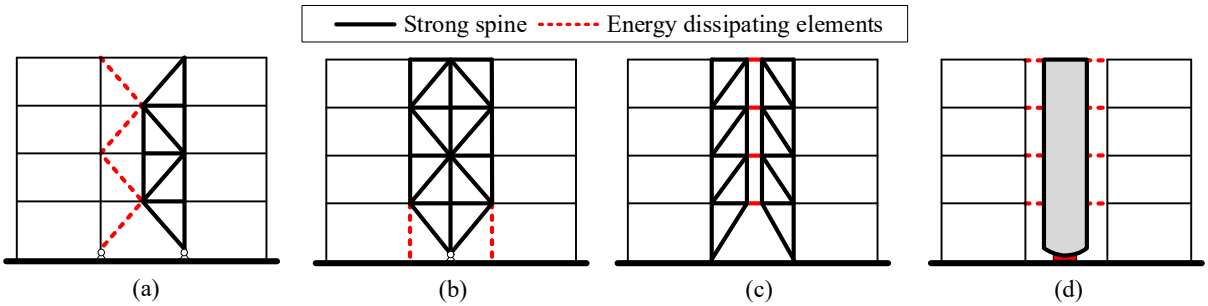

Figure 2. Strong spine systems for steel constructions: (a) Dual BRB frame; (b) Flexural braced frame; (c) Tied braced frame and (d) Pivoting spine.

Design methods have been developed along with the proposal of various strong spine systems and their implementations in real projects. For the strong spines that are part of the original structural system (or have primary elements that are part of the original structural system), such as in dual BRB and flexural braced frames, a strength-based design was usually adopted, in which all the elements in the strong spine are proportioned to have adequate strength to remain elastic under a design basis earthquake (corresponding to 10% probability of exceedance in 50 years in most prescriptive seismic codes) (e.g. Panian et al 2015, Takeuchi et al 2015, Rossi 2007). On the other hand, for the strong spines that are added to an existing structure, a nonlinear time history analysis was usually used to check if the spine remains elastic and to evaluate the effect of drift concentration mitigation (e.g., Qu et al, 2012, Janhunen et al 2013).

For pin-supported walls in moment-resisting frames, Qu et al (2011) investigated the stiffness demand in terms of a stiffness ratio and a drift concentration factor (*DCF*) that was originally used by MacRae et al (2004) for braced steel frames. An empirical equation that relates the demands for the stiffness ratio and the number of stories was proposed, which was later refined by Du and Wu (2014) and Wu and Lu (2015). By assuming an infinitely rigid PS wall, Grigorian and Grigorian (2016) derived a closed-form procedure for the preliminary conceptual design for PS wall-frame dual system. Grigorian et al (2017) further proposed determining the stiffness demand of the PS wall, if it is not infinitely rigid, by limiting its maximum end rotation to a small fraction of the target uniform story drift ratio of the system. Recognizing the importance of the stiffness demand in designing a PS wall, Pan et al (2015) proposed a new stiffness ratio to quantify the relative stiffness of the frame to the wall based on a distributed parameter model consisting of a bending beam for the pin-supported walls and a shear beam for the moment-resisting frame. The analysis suggested that the ratio should generally be less than ten to reduce *DCF* in the building. By the same model, Wu et al (2016) comprehensively investigated the higher mode effect in the PS wall-frame dual system, which would have significant influence on the strength demand for the PS walls,

as will be discussed later in this paper. Sun et al (2018) extended the use of the distributed parameter model to take dampers into account.

A major problem with using the *DCF* as a measure of the adequacy of the PS wall, which has been done in most previous studies regarding the stiffness demand, is the difficulty in assigning a design target. A *DCF* of unity would be an ideal case which would, however, require an impractically, if not infinitely, rigid PS wall. Qu et al (2011) proposed taking the *DCF* corresponding to the first mode shape of the elastic bare frame as a control target, whereas the physical interpretation of this criterion is vague. In this paper, a new parameter with a clearer physical basis is proposed to evaluate the stiffness demand for the PS wall in moment frames. Also, the stiffness demand is described by a new stiffness ratio that captures the mechanical characteristics of a PS wall working together with a moment-resisting frame. Extensive nonlinear dynamic analysis on six prototype reinforced concrete (RC) moment frames is conducted to quantify the stiffness demands. Based on a given stiffness demand, simple criteria for the strength demand for a PS wall considering the higher mode effects are recommended. These recommendations provide a rational basis for proportioning not only PS walls, but also other strong spines in the preliminary design of various strong spine systems.

2. Stiffness ratio and plasticity ratio

2.1. Plasticity ratio

In early studies, the drift concentration factor (*DCF*) was used to evaluate the effect of continuous stiffness in the spreading of story force and lateral drifts, which is defined as the ratio of the maximum to average inter-story drifts (Equation 1, MacRae et al 2004). Although *DCF* is a straightforward measure to show the effect of PS walls in suppressing the lateral drift concentration, a desired extent of uniformness needs to be determined before *DCF* can be used as a quantitative design criterion.

$$DCF = \frac{\theta_{\max}}{u_r/H} \tag{1}$$

where θ_{max} is the maximum inter-story drift ratio along the height, u_r is the roof displacement of the building, and H is the total height of the building.

To avoid such a difficulty, a plasticity ratio, η_p, with clearer physical significance is proposed as a measure to evaluate the effect of PS walls. It is defined as the ratio of the number of plastic hinges in a moment frame, N_p, to that of all column and beam ends where potential hinges can possibly form under earthquakes, N (Equation 2).

$$\eta_p = N_p/N \tag{2}$$

Examples of the two most commonly conceived plastic mechanisms for moment-resisting frames are depicted in Figure 3. In both cases, η_p = 0.5, the total number of possible plastic hinges, N=16, and the number of actual plastic hinges, N_p=8. The PS wall-frame structure would perform equally well no matter if the frame exhibits a beam or a column hinge mechanism in terms of plasticity ratios, although the beam hinge mechanism (Figure 3(a)) is conventionally preferred over the column hinge mechanism (Figure 3(b)) for bare frames to avoid weak story failure. When a PS wall is present and is strong enough to remain essentially elastic, both mechanisms would not lead to weak story failure. By counting the number of plastic hinges, η_p directly represents the portion of a structural system that is mobilized to work against earthquake actions.

The formation of a plastic hinge is determined by the ratio of the curvature at the beam or column ends, ϕ, to the yield curvature of the section, ϕ_y. For the reinforced concrete beam and column members, the yield curvature, ϕ_y, can be calculated by Equation 3 (Qu, 2010), which is an improvement based on the equation proposed by Hernandez-Montes and Aschleim (2003). In this study, it is assumed that a plastic hinge forms when $\phi \geq 1.5\phi_y$.

$$\phi_y = (1.7 + 20\rho_l)(1 - \alpha^2)\frac{\varepsilon_{sy}}{h_0} \tag{3}$$

where ρ_l is the longitudinal reinforcement ratio, α is the axial force ratio, ε_{sy} is the yield strain of the longitudinal rebars, and h_0 is the effective depth of the member.

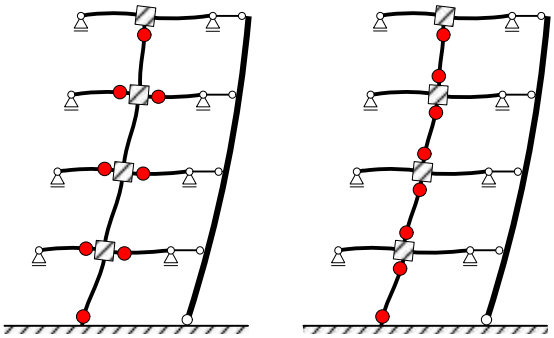

(a) (b)

Figure 3. Hinge locations in (a) a beam hinge mechanism and (b) a column hinge mechanism.

2.2. Stiffness ratio

The first definition of a stiffness ratio to quantify the vertical continuous stiffness in a moment-resisting frame was given by Akiyama and Takahashi (1984). It is the ratio of the inter-story stiffness of the so-called spread column, k_{eq}, to that of the moment-resisting frame, k_R, which are calculated by Equation 4.

$$k_{eq} = \frac{1}{\frac{h^3}{12E_wI_w} + \frac{h}{4G_wA_w}} \tag{4a}$$

$$k_R = \frac{12}{h^2\left(\sum\frac{h}{E_cI_c} + \sum\frac{l}{E_bI_b}\right)} \tag{4b}$$

where h is the story height; E_w, I_w, G_w and A_w are the Young's modulus, moment of inertia, shear modulus and cross-section area of the spread column, respectively; E_c and E_b are the Young's modulus of the columns and beams of the moment frame, respectively; I_c and I_b are the moments of inertia of the columns and beams of the frame, respectively; and l is the span length of the frame.

By assuming that the spread column is infinitely rigid in shear, replacing the inter-story stiffness of a frame, k_R, with that of a braced frame, k, and removing the constant of 12, one gets the frequently used definition of the stiffness ratio for a gravity column in steel braced frames (Equation 5) (MacRae et al 2004, Ji et al 2010).

$$\alpha = \frac{E_wI_w}{kh^3} \tag{5}$$

where E_w and I_w are the Young's modulus and sectional moment of inertia of the gravity columns and k is the story lateral stiffness of the braced frame.

Both of the above definitions are given on a story-by-story basis, whereas the continuous vertical stiffness provided by either the spread column, gravity column or the PS walls is a cross-story property.

In this paper, a global stiffness ratio, β, is defined as the ratio of the stiffness of the wall as an analog of a simply-supported beam under uniformly distributed loads, K_w, to that of the first modal stiffness of the moment frame, K_f (Equation 6). Both K_w and K_f represent global properties of either the wall or the frame, rather than story-by-story properties.

$$\beta = \frac{K_w}{K_f} \tag{6a}$$

$$K_w = \frac{\pi^4E_wI_w}{2H_w^3} \tag{6b}$$

$$K_f = \left(\frac{2\pi}{T_1}\right)^2 M_1 \tag{6c}$$

where E_w, I_w and H_w are the Young's modulus, sectional moment of inertia and height of the PS wall, respectively; M_1 and T_1 are the first mode period and participating mass of the bare frame, respectively. The first mode participating mass is calculated by Equation 7. For preliminary design practice, M_1 can be approximately taken as 85% of the total mass of the bare frame.

$$M_1 = \left(\frac{\{\phi_1\}^{\mathrm{T}}[M]\{1\}}{\{\phi_1\}^{\mathrm{T}}[M]\{\phi_1\}}\right)^2 \{\phi_1\}^{\mathrm{T}}[M]\{\phi_1\} \tag{7}$$

where $[M]$ and $\{\phi_1\}$ are the mass matrix and the first mode shape of the bare frame, respectively.

The analog of a simply-supported beam enables β to be readily applicable to strong spines other than monolithic PS walls, such as steel trusses (Lai and Mahin 2015) and coupled core walls (Janhunen et al 2013). The use of the first modal stiffness as the denominator in the stiffness ratio is also readily extendable when strong spines are used in parallel with other systems such as braced frames (Qu et al, 2014).

It is also worth mentioning that a stiffness ratio, λ, between the shear and flexural stiffness of a distributed parameter model has been proposed to quantify the stiffness of moment-resisting frames (Pan et al 2015), which is represented by a continuous shear beam, relative to the stiffness of the PS wall, which is represented by a continuous flexural beam (Equation 8).

$$\lambda = \sqrt{\frac{KH^2}{E_{\mathrm{w}}I_{\mathrm{w}}}} \tag{8}$$

where K is the distributed stiffness of the frame, which corresponds to the shear force when a unit inter-story drift ratio is applied and has a unit of Newton; H is the total height of the building.

This definition also captures the global nature of a PS wall in spreading inter-story drift over multiple stories. By assuming that $K_{\mathrm{f}}=K/H$ and $H=H_{\mathrm{w}}$, one gets the relationship between β and λ as in Equation 9.

$$\beta = \frac{\pi^4 E_{\mathrm{w}}I_{\mathrm{w}}}{2H^2K} = \frac{\pi^4}{2\lambda^2} \approx \frac{48.7}{\lambda^2} \tag{9}$$

3. Prototype buildings and analysis model

Six prototype RC moment frames of 4, 8 and 12 stories are established for the evaluation of stiffness and strength demands for PS walls. All six frames have the same plan layout (Figure 4), which represents typical classroom buildings in China. They are assumed to be located on a stiff soil site of a 0.4g design-basis spectral pseudo acceleration, that is, in an Intensity VIII region in the Chinese seismic design code (GB 50011-2010, 2010). The story height is 4.1m for the bottom story, 3.8m for the second story, and 3.6m for all other stories for all frames. C40 concrete of 40 MPa nominal compressive strength on 150 mm cubes and HRB400 rebars of 400 MPa nominal yield strength are used. The cast-in-situ RC slabs are 120 mm thick and are reinforced by two layers of 10 mm diameter rebars distributed at 150mm spacing in both directions. A single bay in the frame as is enclosed by dashed lines in Figure 4 is taken as the planar frame prototypes in the following analysis (Figure 5).

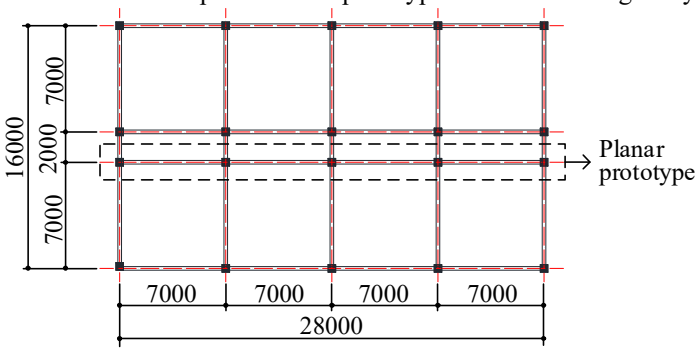

Figure 4. Plan layout of prototype RC frames (unit: mm)

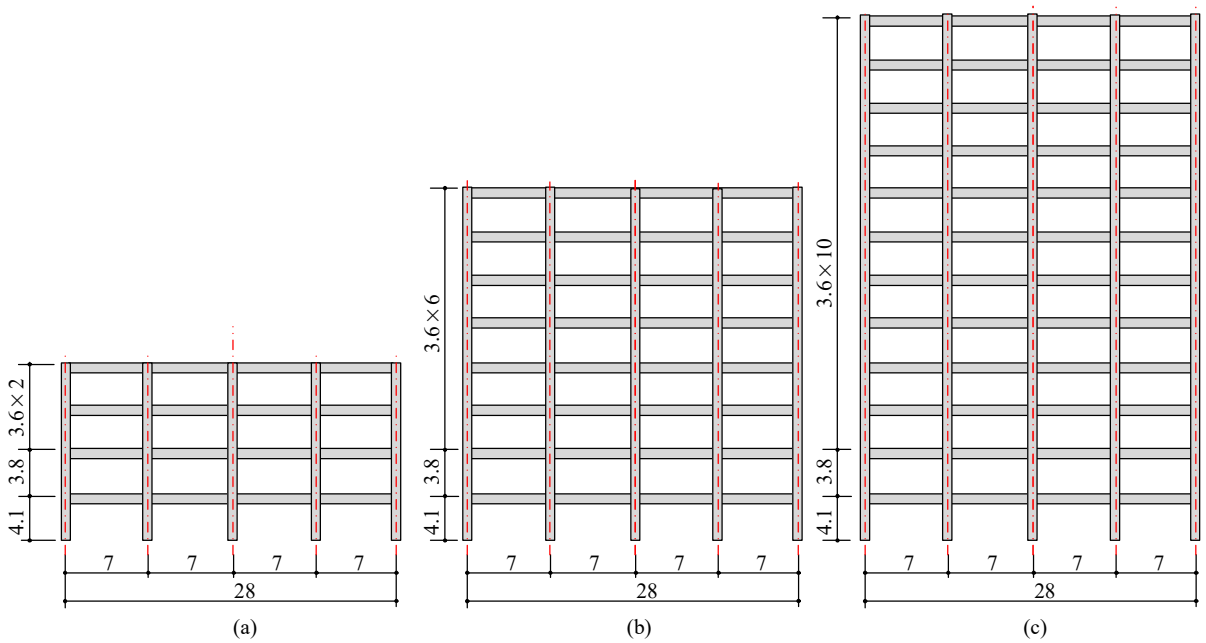

Figure 5. Elevation of prototype planar frames of (a) 4 stories, (b) 8 stories and (c) 12 stories (unit: m).

The prototype moment frames use two different practices in proportioning the beams and columns. One adopts the capacity design that is enforced in the Chinese seismic design codes (GB50011-2010, 2010). In particular, a strong column-weak beam factor, η, is applied to amplify the flexural strength demands for the columns to satisfy Equation 10. The frames that are proportioned by this practice are referred to as strong column-weak beam frames (SC frames), hereinafter.

$$\sum M_{\mathrm{c}} = \eta \sum M_{\mathrm{b}} \tag{10}$$

where ΣM_{c} and ΣM_{b} are the sum of the design moment of columns and that of the beams framing into the same joint. η is the strong column-weak beam factor. For frames located in regions of Intensity VIII, $\eta = 1.7$ for frames taller than 24 m, and $\eta = 1.5$ for other frames as per GB50011-2010 (2010).

In the other practice, the code-stipulated strong column-weak beam requirement is waived. Meanwhile, larger beam and smaller column cross sections are chosen to reduce the column-to-beam stiffness ratios. The resultant frames are referred to as weak column-strong beam frames (WC frames), hereinafter. Although the WC frames do not conform to the current seismic provisions in most seismic regions of the world, they are representative of the existing buildings, especially those designed and constructed before the 1980s when the strong column-weak beam concept was proposed. As aforementioned, the PS wall system is a promising solution for the seismic retrofitting of the WC frames to avoid weak story collapse, even though they do not change the hinge mechanism of the frames, as will be shown in the following discussions. Full details of the prototype frames including the cross-section dimensions and reinforcement are found in Qu et al (2019).

The RC moment frames are modelled in OpenSees (McKenna 2011) by the fishbone model (Nakashima et al 2002) in which the multiple columns in a planar frame are condensed into a single column, and all beams at each floor level are condensed into two half-span beams on both sides of the beam-to-column joint at the same level (Figure 6). The RC frame elements are represented by fiber-sectioned beam elements, in which the RC cross section is divided into many concrete fibers and steel fibers of uniaxial hysteretic behavior. The built-in Concrete02 model in OpenSees, which adopts the Kent-Scott-Park model for the skeleton curve and is capable of modelling both the strength and stiffness deterioration of concrete, is used for the concrete fibers. The fundamental periods of vibration of the six prototype bare frames in their linear elastic state are listed in Table 1. The adequacy of the fishbone model in modelling the nonlinear seismic responses of low- and medium-rise RC frames up to 12 stories was demonstrated in Qu et al (2019). For taller buildings, the global flexural response of the frame may have a nonnegligible effect on the performance of the PS wall-frame system, and more advanced numerical models or a modified fishbone that considers this effect (e.g., Khaloo et al, 2013) should be used.

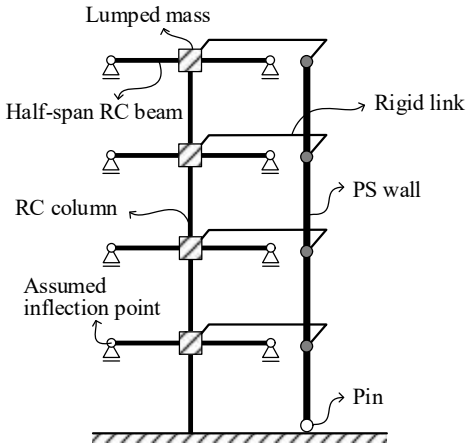

Figure 6. Numerical model in OpenSees for PS wall-frame structure

Table 1. Fundamental periods of prototype bare frames and frames with rigid PS walls (unit: s)

	SC frames		WC frames	
	Bare	w/ rigid PS wall	Bare	w/ rigid PS wall
4-story	0.656	0.618	0.841	0.781
8-story	1.068	1.000	0.988	0.944
12-story	1.656	1.578	1.474	1.435

The PS wall is represented by a linear elastic beam standing parallel and connected to the RC frame by rigid links between the lumped mass of the floor and the wall at each floor level. The wall is supported by an ideal pin at its bottom in the numerical model (Figure 6). The vibration periods of the PS wall-frame systems when the PS wall is infinitely rigid are also listed in Table 1. The introduction of a rigid PS wall only has a marginal effect on the vibration periods. In the following analysis, the sectional stiffness of the PS wall is varied from zero to a very large value to see its effect on the seismic response of the structure. As aforementioned, the PS walls, and other strong spines, are usually used together with energy dissipating devices, which would have an influence on the stiffness and strength demands of the PS walls. For the present paper, energy dissipating devices are not taken into account for simplicity. Their influence will be investigated in further studies.

4. Incremental dynamic analysis and performance target

The incremental dynamic analysis (IDA) is conducted for the prototype moment-resisting frames with PS walls of various stiffness ratios, β. The structures are subjected to two suites of ground motions selected from the PEER ground motion database, that is, a pulse-like ground motion suite of 26 records and a non-pulse like suite of another 26 records. In an IDA, the seismic responses of a building to a set of selected earthquake ground motions, which are scaled incrementally by an intensity measure (IM), are calculated through nonlinear dynamic analysis, and the fragility curve which relates the IM to the probability of exceeding a prescribed damage limit state can be obtained. More details and the implementation of IDA can be found in Vamvatsikos and Cornell (2002). The information of the selected ground motion records is provided in the appendix. The spectral acceleration of 5% damping corresponding to the fundamental period of the frame, $S_a(T_1, 5\%)$, is taken as the intensity measure (IM). All ground motion records are normalized by PGV before they are collectively scaled by the IM for the incremental analysis. The pseudo acceleration spectra of the records which are normalized to have PGV=50cm/s are depicted in Figure 7.

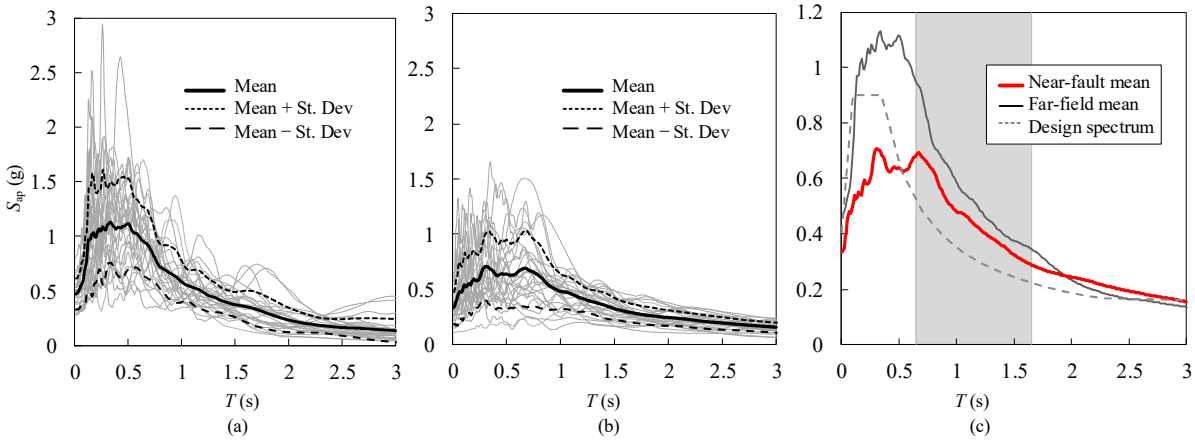

Figure 7. Pseudo acceleration spectra of normalized input ground motion records in (a) non-pulse-like suite, (b) pulse-like suite and (c) a comparison between mean spectra with design spectrum.

With the increase in IM, both the plasticity ratio and the strength demand for a PS wall to remain elastic are expected to increase, although the increase may not be linearly proportional. To provide a consistent basis, a maximum inter-story drift ratio, θ_{max}, of 2%, is taken as the performance target in IDA. This is because (1) it is a commonly-used allowable story drift for buildings under major earthquakes (e.g., ASCE 7-10, 2010), GB50011-2010, 2010) and (2) it is a large enough story drift for moment frames to develop a plastic mechanism so that the plasticity ratio, η_p, can be used to quantify the transition from an inferior local mechanism to a preferred global mechanism. The plasticity ratios and internal force in the elastic PS walls when the frame exhibits a maximum inter-story drift ratio of 2% are taken as the basis for the stiffness and strength demand evaluation in this paper.

The hunt and fill algorithm proposed by Vamvatsikos and Cornell (2004) is used to search for the IM corresponding to the performance target of 2% inter-story drift. The allowable relative error of the IM in searching for the performance target is 1%. The IDA curves of the SC frames taking θ_{max} as the damage measure are depicted in Figure 8 for example. The hollow squares on the IDA curves indicate the performance target points, at which the stiffness and strength demands will be evaluated in the following sections.

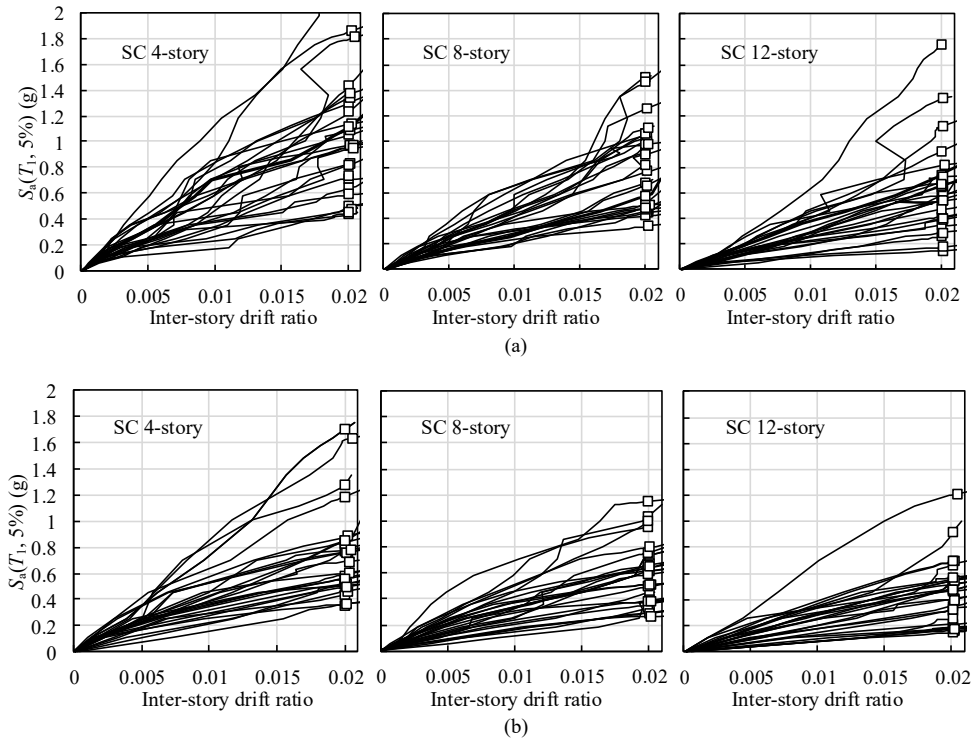

Figure 8. IDA curves for SC frame with β=1 under (a) non-pulse-like and (b) pulse-like ground motions

5 Stiffness demands

The average responses of the IDA results for the 26 ground motion records in a suite, either pulse-like or non-pulse like are further investigated to provide insight into the behavior of the PS wall-frame system.

As have been repeatedly demonstrated in previous studies (Ji et al, 2009 among others), the *DCF*s would decrease significantly as the stiffness ratio increases. This effect is evidently more pronounced for WC frames (dashed lines in Figure 9) which generally exhibit much higher *DCF*s in the absence of a PS wall (i.e. severer drift concentration). The characteristics of the ground motions also affect the *DCF*s. For 4- and 8-story structures, pulse-like ground motions tend to create larger *DCF*s in the structures, while it is the opposite for 12-story structures (Figure 9).

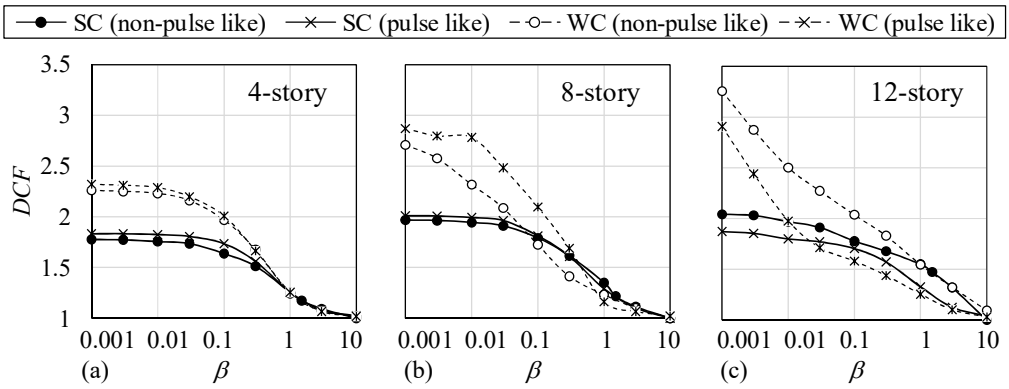

Figure 9. *DCF*-stiffness ratio relationship for (a) 4-story, (b) 8-story and (c) 12-story prototype buildings.

The relationships between the plasticity ratio, η_p, and the stiffness ratio, β, for all prototype structures under both suite of ground motions are summarized in Figure 10. The following can be observed.

(1) In the absence of a PS wall (i.e. $\beta \approx 0$), the WC frames exhibit much lower plasticity ratios than do the SC frames. Under the non-pulse-like motions, for example, the bare frame η_p's are 0.31, 0.36 and 0.43 for the 4-, 8- and 12-story SC frames, respectively, while the η_p's are only 0.22, 0.22 and 0.20 for the corresponding WC frames. Furthermore, the bare frame η_p increases with the number of stories for SC frames, but not for WC frames.

(2) In the absence of a PS wall, η_p is sensitive to ground motion characteristics for both SC and WC frames. For 8-story frames (Figure 10b), for example, the η_p's under the non-pulse-like ground motion suite are 0.36 and 0.22 for the SC and WC frames, respectively. They dropped to 0.27 and 0.18 under the pulse-like ground motion suite even though the maximum inter-story drift ratios are the same (i.e., 2%) in both cases.

(3) With the increase in β (a stiffer PS wall), η_p generally increases for most prototype buildings but in a different manner. For low-rise buildings (e.g., 4-story), the PS wall has practically no effect on η_p until β reaches a threshold beyond which η_p approaches to the ideal 0.5 rapidly (Figure 10a). On the other hand, for taller buildings (e.g., 12-story), the increase in β takes effect in an earlier stage and in a more gradual process (Figure 10c).

(4) As β becomes larger, the difference between the results of the two ground motion suites tends to decrease. When β is large enough to draw η_p close to 0.5, the effect of ground motion characteristics becomes negligible, indicating a more robust structural system against the record-to-record variability.

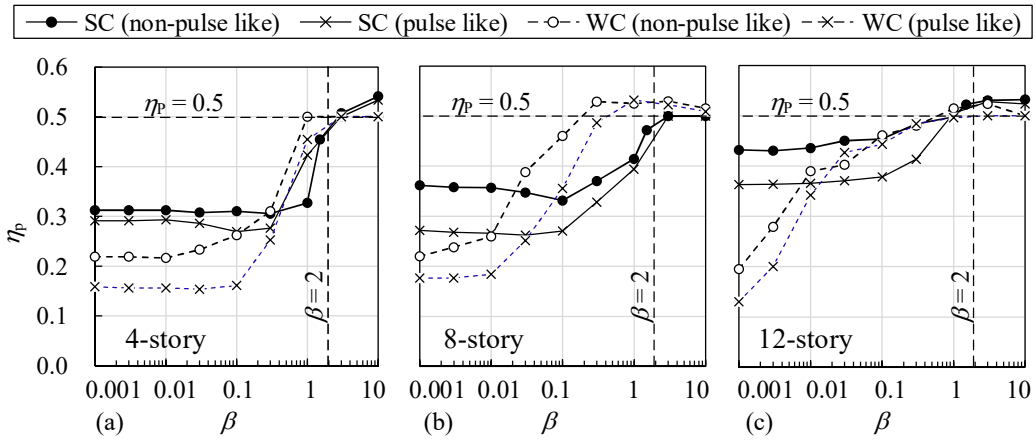

Figure 10. Plasticity ratio-stiffness ratio relationship.

Recall that in the illustrative example in Figure 7, the plasticity ratio, η_p, is 0.5 when a global plastic mechanism forms, no matter if it is a column hinge or a beam hinge mechanism. This is when the seismic capacity of the moment frame is fully mobilized. Although η_p may exceed 0.5 in some cases, especially when multiple-span frames are modelled, an η_p of 0.5 is deemed to be a preferable target for a PS wall to fully activate the different stories in a moment-resisting frame to resist earthquakes. According to the results in Figure 10, the η_p is generally close to or even exceeds 0.5 when β is 2 for all the prototype structures under both suites of ground motions. Therefore, $\beta = 2$ is recommended as a reference value when proportioning PS walls in the preliminary design for a multistory moment frame no matter if it is a strong column or a weak column frame.

It is also interesting to note that Pan et al (2015) suggested a relative stiffness λ of no more than 10 to effectively reduce the *DCF*. According to the approximate relationship between β and λ in Equation 9, this criterion is equivalent to requiring that $\beta \geq 0.485$, which is insufficient to ensure a global plastic mechanism to form in terms of plasticity ratios as shown in Figure 10.

Figure 11 demonstrates the change of plastic hinge mechanism for the 4- and 8-story prototype structures with various β's under the non-pulse-like ground motion suite. When β is negligibly small, the plasticity in both the frames tends to concentrate in the lower stories or some middle stories, depending on the ground motion characteristics. When β=2, all frames developed a global mechanism of η_p=0.5. However, the increase of β would not change a column hinge mechanism into a beam hinge one.

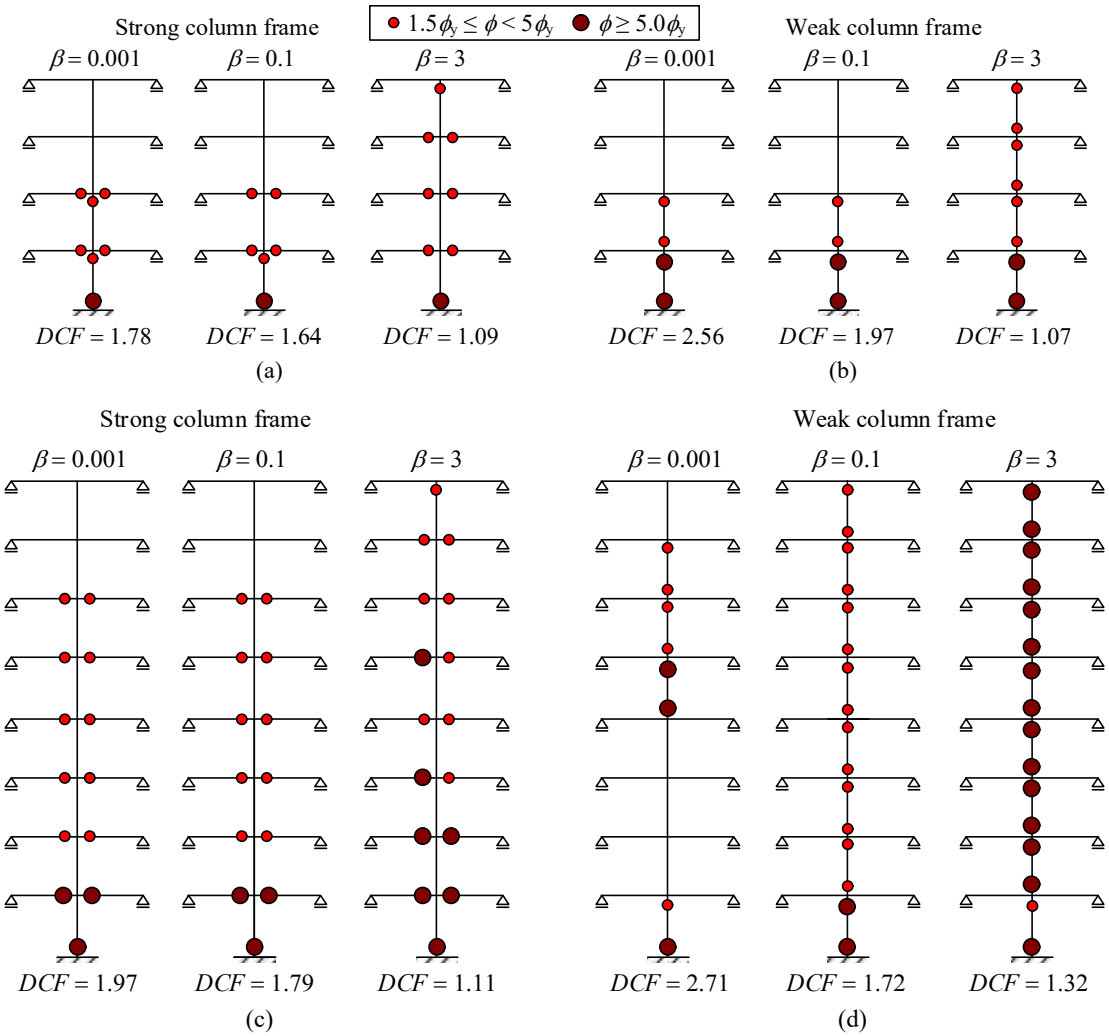

Figure 11. Plastic hinge distribution of (a) a 4-story SC frame, (b) a 4-story WC frame, (c) an 8-story SC frame and (d) an 8-story SC frame at θ_{max} = 2% under non-pulse-like ground motion suite.

The recommended value of $\beta = 2$ is independent of the height of the structures. By its definition, the stiffness ratio, β, has already taken into account the influence of structural height on the stiffness demands of PS walls. By

assuming that the concrete Young's modulus, E_w, the thickness of a PS wall and the number of identical PS walls in a PS wall-frame system are constant, one obtains Equation 11.

$$\beta \propto \frac{d_w^3}{H^3 K_f} \tag{11}$$

where d_w is the cross-sectional depth of the PS wall.

By further assuming that the first mode participating mass, M_1, is proportional to the structural height and T_1=0.0466$H^{0.9}$ as recommended in ASCE 7 (2010) for RC moment-resisting frames, the first mode stiffness, K_f, is inversely proportional to $H^{0.8}$ (Equation 12).

$$K_f = \frac{M_1}{\left(\frac{T_1}{2\pi}\right)^2} \propto \frac{H}{H^{1.8}} = H^{-0.8} \tag{12}$$

By substituting Equation 12 into Equation 11, and with the recommended β of two, which is independent of H, Equation 13 is obtained. It indicates that the required depth of a PS wall to fully mobilize the moment frame grows much more slowly than the total height of the structure (Figure 12).

$$d_w \propto H^{0.73} \tag{13}$$

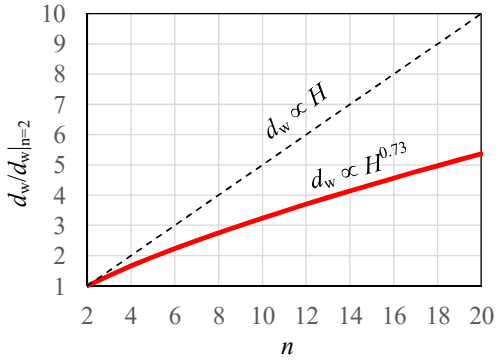

Figure 12. Growth of required PS wall cross sectional depth, d_w, with number of stories, n.

By motivating more structural elements to contribute to the resistance to earthquakes, the PS walls also increase the lateral strength of the structural system, although the walls themselves do not sustain any lateral resistance if there is no frame. Figure 13 depicts the IM at the performance target of 2% maximum inter-story drift of PS wall-frame systems normalized by that of the bare frame. In all cases, the PS walls tend to increase the IM at the performance target. This effect is most significant for tall WC frames under non-pulse like ground motions. When β=2, the PS wall increases the IM at the performance target of the SC frames by approximately 30%-37%, while the increases are 42%, 106% and 142% for the 4-, 8- and 12-story WC frames under non-pulse-like ground motion suites, respectively, and are 54%, 93% and 125% under the pulse-like suite.

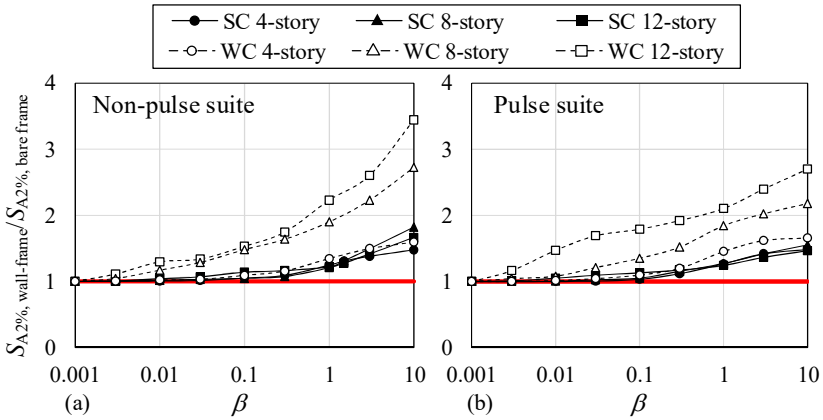

Figure 13. Relationship between increased collapse margin ratios and PS wall stiffness ratios under (a) non-pulse-like ground motions and (b) pulse-like ground motions.

6. Strength demand for pin-supported walls

PS walls are expected to remain elastic so as to maintain the continuous vertical stiffness of the system when the rest of structure may have developed considerable plasticity. The strength demand for PS walls may depend on the following factors.

(1) Performance target. Taking θ_{max} as the DM to define the performance target, the larger the target θ_{max} is, the larger the strength demand is expected for the PS walls. Assuming an elastic PS wall, the maximum internal force in the PS wall in the 8-story SC frame by both the IDA under the JOS000 record and the nonlinear pushover analysis with an inverted triangular lateral force is depicted in Figure 14. In all cases, both the maximum moment and shear force in the PS wall increase with the increase of θ_{max}.

(2) Stiffness ratio. In Figure 14, the internal force in a PS wall of β=3 is several times larger than in a PS wall of β=0.1. The stiffer a PS wall is, the more uniform a lateral drift pattern it tends to impose on the companion moment-resisting frame, and at the same time, the larger internal force it needs to accommodate to remain elastic.

(3) Higher mode effect. It is evident by the example in Figure 14 that a large portion of the strength demand for PS walls is attributed to the higher mode effect, which can be well captured by a dynamic analysis procedure (e.g., IDA) but not by a static pushover analysis. The maximum moment in the PS wall when θ_{max}=2% estimated by an IDA is 2.2 times that by a pushover analysis when β=3, and is 1.9 times when β=0.1. These ratios for the maximum shear force in PS walls are 1.36 when β=3 and 1.4 when β=0.1.

The higher mode effect in a PS wall-frame system was also well documented by Wu et al (2016). In the displacement-based design procedure proposed by Rossi (2007) for tied braced frames, the second mode of vibration is also taken into account in determining the force demand for the braced frame substructures, which serve as strong spines in the system.

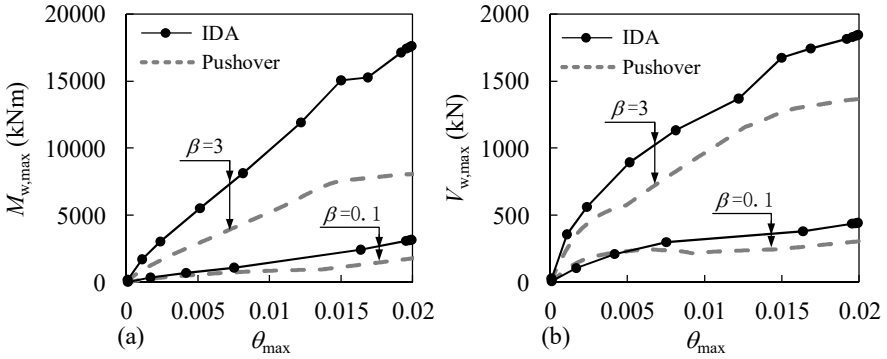

Figure 14. Maximum internal force in PS wall in an 8-story SC frame estimated by different analysis procedures: (a) moment and (b) shear force.

The relationship between the maximum internal force (moment and shear force) in the PS walls and the stiffness ratio, β, is depicted in Figure 15 and 16 based the average results of the aforementioned IDAs. The maximum wall moment, $M_{w,max}$, is normalized by an equivalent over-turning moment of the frame M_o=2/3·WH, where W is the total weight of the structure. The maximum shear force in the wall is normalized by W. The following can be observed: (1) The strength demand increases with a larger β, but the increase rate becomes much smaller beyond a certain value of β; (2) The pulse-like ground motions impose much less strength demands on the PS walls; (3) In most cases, the normalized strength demand is higher for taller buildings.

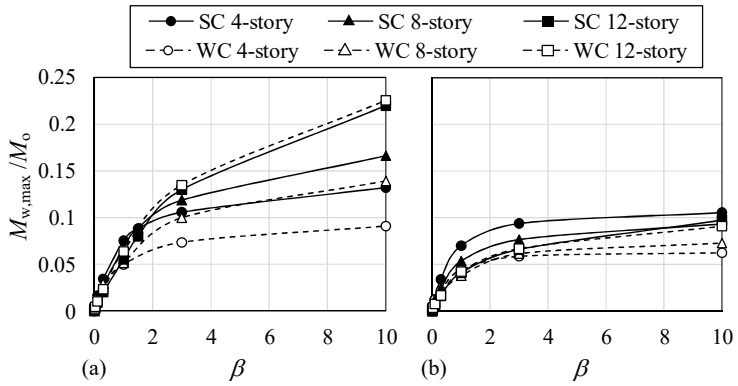

Figure 15. Normalized maximum moment in a PS wall under (a) non-pulse-like ground motions and (b) pulse-like ground motions.

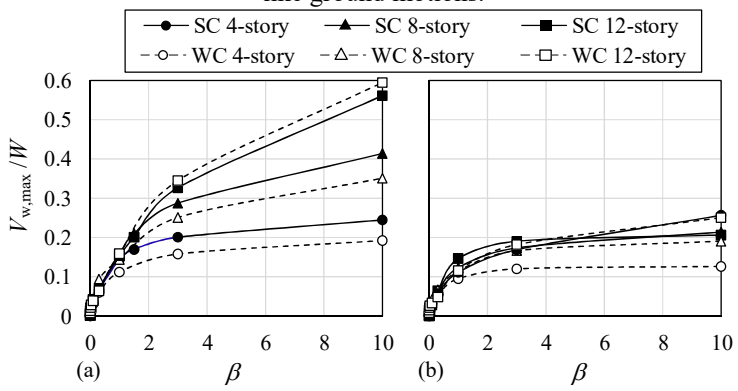

Figure 16. Normalized maximum shear force in a PS wall under (a) non-pulse-like ground motions and (b) pulse-like ground motions.

The normalized maximum internal forces in PS walls of β=2 are summarized in Figure 17. The maximum wall forces are larger when the wall is connected to a SC frame than when it is connected to a WC frame, with the exception of the 12-story structures, in which the latter is slightly larger than the former. For the prototype structures in this study, it is generally conservative to size the PS wall to resist a maximum shear force of $0.25W$ and a maximum moment of $0.1M_o$. The shear force demand is also critical for proportioning the pin support of the wall, because the maximum shear of the PS wall is very likely to take place at the base.

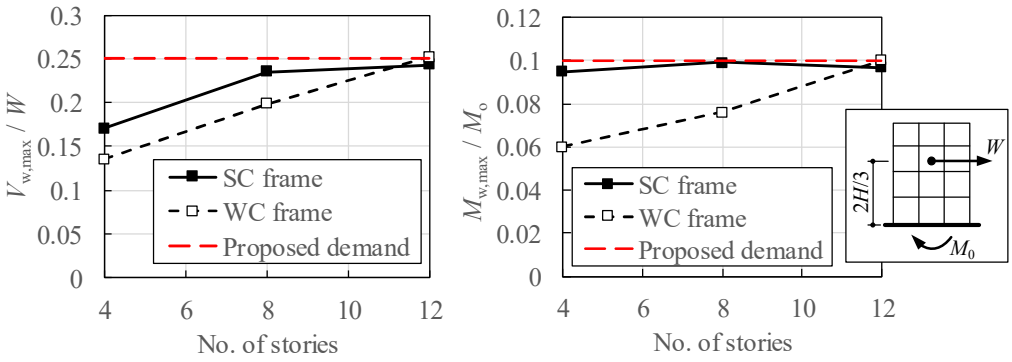

Figure 17. Normalized maximum force in PS wall when β=2 under non-pulse-like suite: (a) shear and (b) moment.

The analogy between a PS wall and a simply supported beam under uniformly distributed load, based on which the stiffness ratio, β, is proposed, is assured by the internal force distribution of the prototype structures (Figure 18). The distributions shown in Figure 18 are the average of results corresponding to the ground motions in the non-pulse-like suite at the 2% inter-story drift performance target. When the wall is slender and β is low, both the shear force and moment distributions exhibit large scattering among different prototype buildings, and deviate significantly from the ideal force distribution in a simply supported beam under uniformly distributed load. With the increase in β, the scattering decreases and the distributions become very close to those of a simple supported beam.

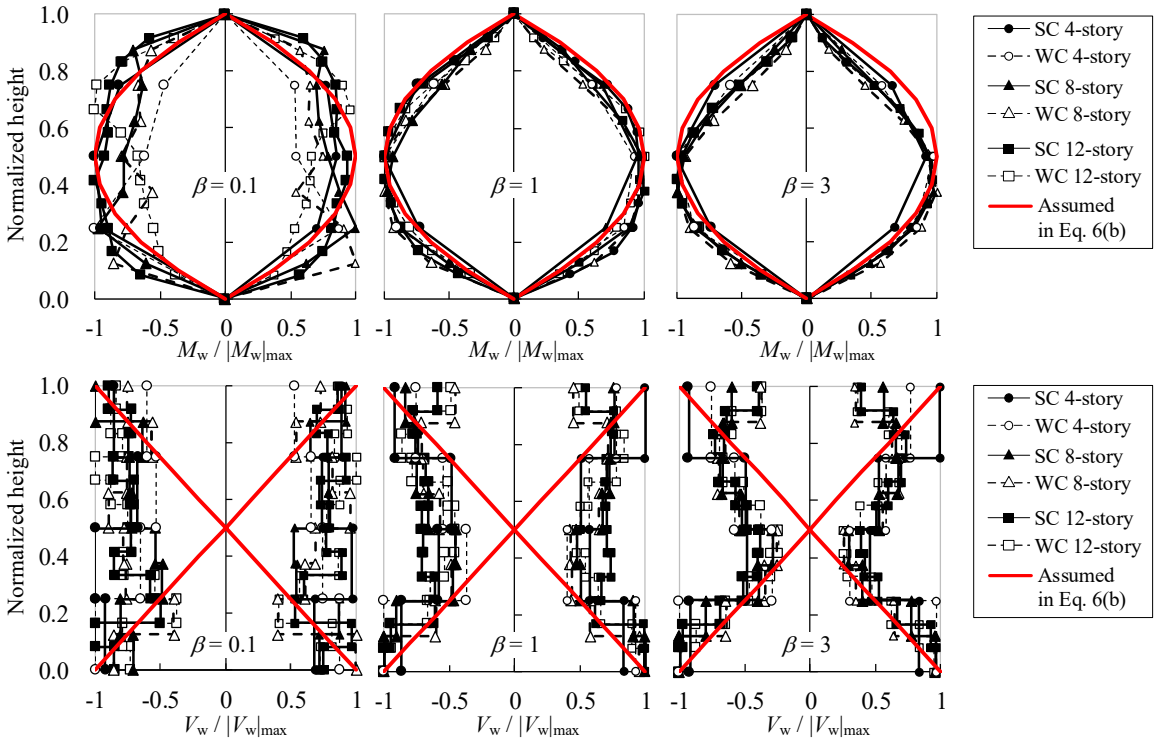

Figure 18. Force distributions in PS walls.

7. Conclusions

Among a variety of strong spines in various constructions, pin-supported walls are effective in redistributing lateral drifts among different stories of RC frames and thus mitigating the weak story failure. To evaluate this effect on a rational basis, a plasticity ratio is proposed that directly represents the portion of the moment frame that is mobilized. The influence of the PS wall stiffness on the plasticity ratio is investigated by incremental dynamic analysis on six multi-story prototype frames equipped with PS walls of various stiffness. The corresponding strength demand for the PS walls is also extracted. The following conclusions can be drawn from the results.

(1) The newly-defined stiffness ratio, β, provides a consistent measure of the relative stiffness of PS walls to RC frames and inherently takes into account the influence of the overall structural height on the stiffness demands for PS walls.

(2) A stiffness ratio of $\beta = 2$ can generally ensure a global plastic mechanism by making the plasticity ratio close enough to 50%. This is valid for both strong column and weak column frames of various numbers of stories under both pulse-like and non-pulse-like ground motions.

(3) PS walls can also increase the lateral strength of a moment-resisting frame, although the walls themselves do not sustain any lateral resistance if there is no frame.

(4) Higher mode vibration has a significant effect on the strength demand of PS walls. The static analysis procedure may greatly underestimate the force in PS walls, and possibly in other strong spines as well.

(5) The strength demands for PS walls tend to be larger in strong-column RC frame and when under non-pulse-like ground motions.

(6) For the prototype structures in the current study, a shear force of $0.25W$ and a moment of $0.1M_o$ represent a conservative strength demand for a PS wall of $\beta = 2$.

It should be noted that PS walls usually work together with additional energy dissipating devices. The influence of these devices is not taken into account in the current study and deserves further investigation.

Data Availability Statement

Some data, models, or codes that support the findings of this study are available from the corresponding author upon reasonable request. They include the full details and OpenSees models of the prototype planar frames, the incremental dynamic analysis results and the corresponding hinge ratios.

Acknowledgements

This work was jointly supported by the Scientific Research Fund of the Institute of Engineering Mechanics, China Earthquake Administration (Grant No. 2016A05) and the National Natural Science Foundation of China (Grant No. 51478441).

References:

Akiyama H, Takahashi M (1984). Ds-values for damage-dispersing type multi-story frames. *Journal of Structural and Construction Engineering Transaction of AIJ*, 341: 54–61 (in Japanese).

Ancheta TD, Darragh RB, Stewart JP, et al (2004). Strengthening of moment-resisting frame structures against near-fault ground motion effects. *Earthquake Engineering and Structural Dynamics*, **33**(6): 707-720.

ASCE 7-10 (2010). *Minimum design loads for buildings and other structures*.

Aoki K, Fukuyama K, Okumoto H, Ukai K, Taga K (1998). Design of a high rise building using unbonded braces with varying cross section. *Journal of Construction Steel*, 6: 139-144 (in Japanese).

Du YF, Wu DY (2014). Performance analysis of light energy dissipative rocking frame designed on the basis of stiffness demand. *China Civil Engineering Journal*, **47**(1): 24-35 (in Chinese).

GB 50011-2010 (2010). *Code for Seismic Design of Buildings*. Beijing (in Chinese).

Grigorian CE, Grigorian M (2016). Performance control and efficient design of rocking-wall moment frames. *Journal of Structural Engineering, ASCE*, **142**: 04015139.

Grigorian, M, Moghadam AS, Mohammadi H (2017). Advances in rocking core-moment frame analysis. *Bulletin of Earthquake Engineering*, 15(12): 5551-5577. DOI: 10.1007/s10518-017-0177-8.

Hernandez-Montes E, Aschleim M (2003). Estimates of the yield curvature for design of reinforced concrete columns. *Magazine of Concrete Research*, **55**(4): 373-383.

Janhunen B, Tipping S, Wolfe J (2013). Seismic retrofit of a 1960s steel moment-frame highrise using a pivoting spine. *SEAOC 2013 Convention Proceedings*, San Diego, September 18-21.

Ji XD, Kato M, Wang T, Hitaka T, Nakashima M (2009). Effect of gravity columns on mitigation of drift concentration for braced frames. *Journal of Constructional Steel Research*, **65**(12): 2148-2156.

Khaloo AR and Khosravi H (2013). Modified fish-bone model: A simplified MDOF model for simulation of seismic responses of moment resisting frames. *Soil Dynamics and Earthquake Engineering*, **55**: 195–210.

Kishida T, Donahue JL (2013). *PEER NGA-West2 Database*. Pacific Earthquake Engineering Research Center, Report 2013/03. [http://ngawest2.berkeley.edu/].

Lai JW, Mahin SA (2015). Strongback system: a way to reduce damage concentration in steel-braced frames. *Journal of Structural Engineering, ASCE*, **141**(9).

Liu J (2017). Strongback steel-braced frames for improved seismic behavior in buildings. *Engineering Journal*, **21**: 297-307.

MacRae G A, Kimura Y, Roeder C (2004). Effect of column stiffness on braced frame seismic behavior. *Journal of Structural Engineering*, ASCE, **130**(3): 381-391.

McKenna F (2011). OpenSees: A framework for earthquake engineering simulation. *Computer Science and Engineering*, **13**(4): 58–66.

Nakashima M, Ogawa K, Inoue K (2002). Generic Frame Model for Simulation of Earthquake Responses Analysis, *Earthquake engineering and structural dynamics*, **31**(3): 671-692.

Pan P, Wu SJ, Nie X. A (2015). distributed parameter model of a frame pin-supported wall structure. *Earthquake Engineering and Structural Dynamics*, **44**: 1643-1659.

Panian L, Bucci N, Janhunen B (2015). BRBM frames: an improved approach to seismic-resistant design using buckling-restrained braces. *Proc. 2nd ATS&SEI Conference on Improving the Seismic Performance of Existing Buildings and Other Structures*, San Francisco, December 10-12: 632-643.

Paulay T, Priestley MJN (1992). *Seismic design of reinforced concrete and masonry buildings*. John Wiley & Sons, Inc: New York: 500–516.

Pollino M, Slovenec D, Qu B, Mosqueda G. Seismic rehabilitation of concentrically braced frames using stiff rocking cores. *Journal of Structural Engineering, ASCE*, **143**(9): 2017.

Qu B, Sanchez-Zamora F, Pollino M (2014). Mitigation of inter-story drift concentration in multi-story steel concentrically braced frames through implementation of rocking cores. *Engineering Structures*, **70**: 208-217.

Qu Z, Wada A, Ye LP (2011). Seismic retrofit of frame structures using rocking wall system. *Journal of Building Structures*, **32**(9): 11-19 (in Chinese).

Qu Z, Wada A, Motoyui S, Sakada H, Kishiki S (2012). Pin-supported walls for enhancing the seismic performance of building structures. *Earthquake Engineering and Structural Dynamics*, **41**(14): 2075-2091.

Qu Z, Sakata H, Midorikawa S, Wada A (2015). Lessons from the behavior of a monitored eleven-story building during the 2011 Tohoku-oki earthquake for robustness against design uncertainties. *Earthquake Spectra*, **31**(3): 1471-1492.

Qu Z, Gong T, Li QQ, Wang T (2019). Evaluation of the fishbone model in simulating the seismic response of

multistory reinforced concrete moment-resisting frames. *Earthquake Engineering and Engineering Vibration*, **18**(2): 315-330.

Rossi PP (2007). A design procedure for tied braced frames. *Earthquake Engineering & Structural Dynamics*, **36**: 2227-2248.

Slovenec D, Sarebanha A, Pollino M, Mosqueda G, Qu B (2017). Hybrid testing of the stiff rocking core seismic rehabilitation technique. *Journal of Structural Engineering, ASCE*, **143**(9).

Sun TS, Kurama YC, Zhang PZ, Ou JP (2018). Linear-elastic lateral load analysis and seismic design of pin-supported wall-frame structures with yielding dampers. *Earthquake Engineering & Structural Dynamics*, DOI: 10.1002/eqe.3002.

Takeuchi T, Suzuki K (2003). Performance-based design for truss-frame structures using energy dissipation devices. *Proc. Behavior of Steel Structures in Seismic Area (STESSA)*, Naples, Italy: 55-61.

Takeuchi T, Chen XC, Matsui R (2015). Seismic performance of controlled spine frames with energy-dissipating members. *Journal of Constructional Steel Research*, 114: 51-65.

Tremblay R, Ben FM, Sabelli R (2004). An innovative bracing configuration for improved seismic response. *Proc. Recent Advances and New Trends in Structural Design International Colloquium*. Timisoara, Romania: 419-430.

Tremblay R, Merzouq S (2004). Dual buckling restrained braced steel frames for enhanced seismic response. *Proc. Passive Control Symposium*, Yokohama, November, 15-16: 89-104.

Tremblay R, Chen L, Tirca L (2014). Enhancing the seismic performance of multi-storey buildings with a modular tied braced frame system with added energy dissipating devices. *International Journal of High-Rise Buildings*, **3**(1): 21-23

Wada A, Qu Z, Ito H, Motoyui S, Sakata H, Kasai K (2009). Seismic retrofit using rocking walls and steel dampers. *Proc. ATC/SEI Conference on Improving the Seismic Performance of Existing Buildings and Other Structures*, San Francisco, US.

Vamvatsikos D and Cornell CA (2002). Incremental dynamic analysis, *Earthquake Engineering and Structural Dynamics*, **31**(3), 2002: 491-514.

Vamvatsikos D and Cornell CA (2004). Applied incremental dynamic analysis. *Earthquake Spectra*, **20**(4): 523-553.

Wu DY, Lu XL (2015). Structural performance evaluation of a new energy-dissipation and light-weight rocking frame by numerical analysis and experiment. *Proc. 10th Pacific Conference on Earthquake Engineering*, Sydney, November, 6-8: Paper No.191.

Wu SJ, Pan P, Zhang DB (2016). Higher mode effects in frame pin-supported wall structure by using a distributed parameter model. *Earthquake Engineering & Structural Dynamics*, **45**(14): 2371-2387.

Appendix

Table A. Near-fault ground motion records

ID	Earthquake	Station	File Name	PGA (g)	PGV (cm/s)
1	Imperial Valley-06	El Centro Array #5	H-E05230	0.3785	90.45
2	Imperial Valley-06	El Centro Array #6	H-E06140	0.4105	64.80
3	Imperial Valley-06	El Centro Array #7	H-E07140	0.3375	47.56
4	Nahanni, Canada	Site 2	S2330	0.3226	33.10
5	Superstition Hills-02	Parachute Test Site	B-PTS225	0.4550	111.89
6	Loma Prieta	LGPC	LGP000	0.9663	108.57
7	Loma Prieta	LGPC	LGP090	0.5872	47.01
8	Loma Prieta	Saratoga - Aloha Ave	STG000	0.5125	41.12
9	Loma Prieta	Saratoga - W Valley Coll.	WVC000	0.2551	42.41
10	Loma Prieta	Saratoga - W Valley Coll.	WVC270	0.3322	61.50
11	Erzican, Turkey	Erzincan	ERZ-EW	0.4955	64.25
12	Erzican, Turkey	Erzincan	ERZ-NS	0.5153	83.88
13	Cape Mendocino	Petrolia	PET000	0.5896	48.28
14	Cape Mendocino	Petrolia	PET090	0.6624	90.07
15	Landers	Lucerne	LCN260	0.7268	146.62
16	Northridge	Newhall - Fire Station	NWH360	0.5898	97.68
17	Northridge	Rinaldi Receiving Station	RRS228	0.8252	160.16
18	Northridge	Rinaldi Receiving Station	RRS318	0.4865	74.52
19	Northridge	Sylmar - Olive View Med FF	SYL360	0.8433	130.24
20	Kobe	KJMA	KJM000	0.8213	81.55
21	Kocaeli	Yarimca	YPT060	0.2677	65.67
22	Kocaeli	Yarimca	YPT330	0.3490	62.12
23	Chi-Chi	TCU052	TCU052	0.3482	158.88
24	Chi-Chi	TCU065	TCU065-E	0.8138	126.09
25	Chi-Chi	TCU068	TCU068	0.5660	176.49
26	Duzce	Duzce	DZC270	0.3481	59.93

Table B. Non-pulse-like ground motion records

ID	Earthquake	Station	File Name	PGA (g)	PGV (cm/s)
1	Friuli, Italy-01	Tolmezzo	A-TMZ000	0.3513	22.02
2	Friuli, Italy-01	Tolmezzo	A-TMZ270	0.3148	30.78
3	Imperial Valley-06	Delta	H-DLT262	0.2378	25.98
4	Imperial Valley-06	Delta	H-DLT352	0.3511	32.99
5	Loma Prieta	Hollister Diff. Array	HDA165	0.2687	43.84
6	Loma Prieta	Hollister Diff. Array	HDA165	0.2789	35.53
7	Loma Prieta	Sunnyvale - Colton Ave.	SVL270	0.2073	37.24
8	Loma Prieta	Sunnyvale - Colton Ave.	SVL360	0.2086	36.01
9	Cape Mendocino	Rio Dell Overpass - FF	RIO270	0.3854	43.78
10	Cape Mendocino	Rio Dell Overpass - FF	RIO360	0.5489	42.04
11	Landers	Joshua Tree	JOS000	0.2737	27.47
12	Landers	Joshua Tree	JOS090	0.2840	43.36
13	Northridge-01	Canyon Country	LOS000	0.4100	42.98
14	Northridge-01	Canyon Country	LOS270	0.4820	45.37
15	Northridge-01	Castaic - Old Ridge Route	ORR090	0.5683	52.54
16	Northridge-01	Castaic - Old Ridge Route	ORR360	0.5143	52.17
17	Northridge-01	LA - Saturn St	STN020	0.4745	34.44
18	Northridge-01	LA - Saturn St	STN110	0.4386	39.11
19	Kobe, Japan	Kakogawa	KAK000	0.2514	18.76
20	Kobe, Japan	Kakogawa	KAK090	0.3447	27.64
21	Kobe, Japan	Shin-Osaka	SHI000	0.2432	37.84
22	Kobe, Japan	Shin-Osaka	SHI090	0.2119	27.92
23	Chi-Chi, Taiwan	CHY034	CHY034-N	0.3097	48.47
24	Chi-Chi, Taiwan	CHY034	CHY034-W	0.2485	38.81
25	Hector Mine	Hector	HEC000	0.2656	28.56
26	Hector Mine	Hector	HEC090	0.3368	41.72